Swift/BAT and MAXI/GSC Broadband Transient Monitor

Takanori Sakamoto¹, Ryoma Oda¹, Tatehiro Mihara², Atsumasa Yoshida¹, Makoto Arimoto³, Scott D. Barthelmy⁴, Nobuyuki Kawai³, Hans A. Krimm^{4,5,6}, Satoshi Nakahira⁷ and Motoko Serino²

Received; Accepted

Abstract

We present the newly developed broadband transient monitor using the *Swift* Burst Alert Telescope (BAT) and the *MAXI* Gas Slit Camera (GSC) data. Our broadband transient monitor monitors high energy transient sources from 2 keV to 200 keV in seven energy bands by combining the BAT (15-200 keV) and the GSC (2-20 keV) data. Currently, the daily and the 90-minute (one orbit) averaged light curves are available for 106 high energy transient sources. Our broadband transient monitor is available to the public through our web server, http://yoshidalab.mydns.jp/bat_gsc_trans_mon/, for a wider use by the community. We discuss

¹College of Science and Engineering, Department of Physics and Mathematics, Aoyama Gakuin University, 5-10-1 Fuchinobe, Chuo-ku, Sagamihara-shi, Kanagawa 252-5258

²MAXI team, RIKEN, 2-1 Hirosawa, Wako, Saitama, 351-0198

³Department of Physics, Tokyo Institute of Technology, 2-12-1 Ookayama, Meguro-ku, Tokyo 152-8851

⁴NASA Goddard Space Flight Center, Greenbelt, MD 20771, USA

⁵Center for Research and Exploration in Space Science and Technology (CRESST), NASA Goddard Space Flight Center, Greenbelt, MD 20771, USA

⁶Universities Space Research Association, 7178 Columbia Gateway Drive, Columbia, MD 21046 USA

⁷JEM Mission Operations and Integration Center, Human Spaceflight Technology Directorate, Japan Aerospace Exploration Agency, 2-1-1 Sengen, Tsukuba, Ibaraki 305-8505

^{*}E-mail: tsakamoto@phys.aoyama.ac.jp

the daily sensitivity of our monitor and possible future improvements to our pipeline.

Key words: methods: data analysis — stars: activity — binaries: general – stars: black holes — stars: jets

1 Introduction

High energy astrophysical sources show a temporal variability in a broad spectral range. The X-ray (1-10 keV) and hard X-ray ranges (10-100 keV) are especially important observing windows to understand the temporal characteristics of high energy sources which involve spectral changes. For instance, a black hole candidate shows state changes in its flux and spectrum; in the quiescent state the X-ray emission is dominated by the hard emission, whereas in outburst the soft emission from the accretion disk becomes dominate. Some low mass X-ray binaries produces bright bursts in X-rays, so called X-ray bursts, which are caused by thermonuclear flashes of accreting material on the surface of the neutron star. An accreting X-ray binary pulsar sometimes shows intense outbursts in X-rays when the neutron star passes the disk or dense stellar wind of its companion. Cyclotron resonance lines, one of the direct observational approaches to measure the magnetic field of a neutron star, are most easily observable in the hard X-ray range from binary pulsar during outburst. An isolated neutron star with a high magnetic field, a so called magnetar, occasionally shows an outburst with multiple short duration bursts in hard X-rays believed originate from a large release of its internal magnetic energy. The time-domain astronomy which has been revolutionized by *Swift* (Gehrels et al. 2004) has become a frontier field of astronomy.

The Burst Alert Telescope (BAT; Barthelmy et al. 2005) onboard *Swift* has been monitoring the hard X-ray sky (14-200 keV) thanks to its wide field of view since 2004. On the other hand, the Gas Slit Camera (GSC; Mihara et al. 2011) on the *MAXI* mission (Matsuoka et al. 2009) has been observing the sky in softer energy band (2-30 keV) since 2009. Both instrument teams are providing the light curve data in real-time to the public (Krimm et al. 2013; Sugizaki et al. 2011). However, the Swift/BAT transient monitor¹ (Krimm et al. 2013) is limited to a single energy band of 15-50 keV because the pipeline is using the data extracted in a single 15-50 keV band on-board (the data product called the BAT scaled-map data). Furthermore, there is no realtime transient monitor producing light curves in the full dynamic range of the BAT and the GSC data with the same time axis. By combining the data of the BAT and the GSC, we are able to construct broadband light curves of high energy

http://swift.gsfc.nasa.gov/results/transients/

transient sources with a high scientific merit. For example, the spectral state changes of several black hole candidates are investigated intensively using the BAT and the GSC data (XTE J1752–223, e.g., Nakahira et al. 2010; Swift J1753.5–0127, e.g., Yoshikawa et al. 2015; Swift J1910.2–0546, e.g., Nakahira et al. 2014; GX 339–4, e.g., Shidatsu et al. 2011b). The state transition of bright low-mass X-ray binaries have also been studied in detail using both BAT and GSC data (e.g., Asai et al. 2015.). Using both the *MAXI* and the *INTEGRAL* data, there is the web page for monitoring X-ray and hard X-ray activities of high-mass X-ray binaries.² Therefore there is a great demand to gather broad band light curves of high-energy transient sources from multiple missions and present them in a consistent format along a single time axis.

In this paper, we introduce the broadband transient monitor utilizing the BAT and GSC data. This transient monitor covers the dynamic range from 2 keV to 200 keV, which is ideal to monitor high energy transients in a broad spectral coverage.

The paper is organized as follows. We present the analysis method in §2. In §3, our broadband transient monitor is introduced. We further discuss our broadband transient monitor in §4.

2 Analysis

The flowchart of our pipeline is shown in Figure 1. As the initial step to construct the broadband transient monitor, independent pipelines were developed just to mirror the *Swift* BAT data to our server. This step is rather crucial for the entire process because it takes a significant amount of time to download the BAT data from the *Swift* data archive center in the U.S. (Swift Data Center (SDC) ³ and HEASARC⁴) to Japan. Since the *Swift* data are initially stored at the SDC, and then, archived to the HEASARC seven days after the observation, two separate pipelines were developed to mirror both SDC and HEASARC data, which are available to the public from our web server (the SDC data mirror⁵ and the HEASARC data mirror⁶) located in Japan. Note that only the Swift/BAT related data are mirrored from the HEASARC to our server. The script to mirror the SDC data is running once an hour, whereas the script to mirror the HEASARC archive runs once a day.

The basic BAT data analysis is performed using the HEASOFT software package. The batsurvey script is used to process the BAT survey (Detector Plane Histogram (DPH)) data. The default eight energy bands (14-20 keV, 20-24 keV, 24-35 keV, 35-50 keV, 50-75 keV, 75-100 keV,

² http://integral.esac.esa.int/bexrbmonitor/webpage_oneplot.php

³ http://swift.gsfc.nasa.gov/cgi-bin/sdc/ql?

⁴ http://heasarc.gsfc.nasa.gov/FTP/swift/data/obs/

 $^{^{5}}$ http://yoshidalab.mydns.jp/swift_sdc_ql/

⁶ http://yoshidalab.mydns.jp/swift_bat_heasarc/

100-150 keV and 150-195 keV) and the original time resolution of the DPH data (timesep = "DPH") were specified in the script. The typical exposure time of the original DPH data is five minutes. Products are made for 146 sources which were flagged as bright hard X-ray sources in the BAT 70 month all-sky hard X-ray survey (Baumgartner et al. 2013). The data after August 2009, when *MAXI* and *Swift* operations overlap, were processed. The batsurvey script produces so-called 'level 2' catalogs for each source, which contain the extracted count-rate and the incident angle of the source. Once the batsurvey process is completed, all the level 2 catalogs (final outputs of the batsurvey script) are merged using batsurvey-catnum script and time sorted by ftsort for all 146 sources.

The BAT count rates extracted by the batsurvey script must be corrected for the energy dependent vignetting of incoming photons (Tueller et al. 2010). To model this off-axis effect in the count rate at each energy band, we processed the survey data between 2004 and 2005, when the Crab nebula was in the field of view at various incident angles. Figure 2 illustrates the significant energy dependent systematic effect between the Crab count rate and incident angle in the 15-20 keV and the 100-150 keV band, as an example. A quadratic function was used to fit the trend between the count rate and the incident angle for all eight energy bands (Table 2). In each band, the count rate is corrected by the rate of the on-axis Crab rate to the estimated Crab rate at the given incident angle. Next, the original eight energy bands are binned to four energy bands (14-24 keV, 24-50 keV, 50-100 keV and 100-195 keV). And then, a one day averaged and a 90-minutes (1 orbit) averaged light curves are generated using rebingauss1c.

The *MAXI* GSC one day and 90 minutes light curves are downloaded from the *MAXI* public web page⁷ for the common sources of the BAT 146 bright sources in the input catalog of the BAT data process and the 369 (as of July 2015) sources listed in the *MAXI* public web page. The number of common sources in the current monitor is 106. This limitation mainly comes from the number of sources in the BAT input catalog. However, since all the created BAT sky images are stored in our computer, only the source extraction tool, batcelldetect, is needed to run through all the archival images to add a new source from the BAT data. We have a plan to add the sources which were detected in outburst in the BAT transient monitor (Krimm et al. 2013) in the past six years to our transient monitor pipeline.

The light curves of the BAT and the GSC are combined and plots are generated using the python matplotlib module.⁸ The BAT light curve data are available in FITS format. The interactive light curve based on the python mpld3 module⁹ is also available, so that a user can move and zoom-in

⁷ www.maxi.riken.jp

⁸ http://matplotlib.org

⁹ http://mpld3.github.io

3 BAT and GSC Broadband Transient Monitor

Our broadband transient monitor is available to the public from the web server at Aoyama Gakuin University: http://yoshidalab.mydns.jp/bat_gsc_trans_mon/. Currently, the broadband light curves of 106 known sources are accessible from the web page. The web page updates \sim 3 times a day depending on the amount of the data which need to be processed. The products of our BAT-GSC broadband transient monitor are summarized in Table 3.

Here, we highlight the products of several sources in our broadband transient monitor. Figure 3 and 4 show our broadband light curves of the black hole binaries Cygnus X-1 and GRS 1915+105. Those light curves clearly show multiple spectral state transitions between "low-hard" and "high-soft" states, which are believed to indicate a change in the geometry of the accretion disk (e.g., Esin et al. 1997). For example, the last clear state change was happening around MJD 57125 for Cygnus X-1 and around MDJ 56252 for GRS 1915+105. As can be seen in the light curves, the borderline energy which the emission becomes brighter or dimmer when the source is in the high-soft state is around 10 keV for Cygnus X-1 and 15 keV for GRB 1915+105. Figure 5 shows the long-term temporal behavior of GX 339-4, a Galactic transit black hole with a low-mass companion. During the giant outburst in the year 2010 (e.g., MJD 55200-55600), the burst emission showed a strong hard-to-soft evolution. The initial hard emission was visible up to the highest energy band of 100-195 keV. This hard X-ray emission episode is dominated by Comptonized photons from the accretion disk (e.g., Shidatsu et al. 2011a).

The γ -ray blazar, Mrk 421, showed several flares visible up to 100 keV (Figure 6). Since the BAT energy range is located at the dip between the two broad peaks in the spectral energy distribution of Mrk 421 (e.g., Abdo et al. 2011), the BAT hard X-ray emission is not that evident compared to the soft X-ray band of the GSC. However, during the outburst, the hard X-ray emission is clearly visible in the BAT data, and the broad-spectral properties of the source can be investigated using our monitor. Figure 7 shows the light curve of the Seyfert 1.5 galaxy NGC 4151 which has a hard continuum in its spectrum (Keck et al. 2015). Unlike previous examples, its emission and the temporal variability are clearly visible in the BAT data rather than the GSC data.

In Figure 8, the several giant outburst episodes are visible in the broadband light curve of a high-mass X-ray pulsar A0535+262. Since the emission during the giant outbursts were so intense, the temporal profile up to 100 keV is clearly visible even in the one orbit light curve (right panel of Figure 8). A recent study showed that the energy of the cyclotron resonance line of A0535+262,

which was found typically around 45 keV, increased when the flux was high (Sartore et al. 2015). Thus, it is important to monitor those cyclotron sources in a broad energy band to understand the transient spectral features in various flux levels. As can be seen in those examples, our transient monitor includes various types of sources and can monitor interesting temporal and spectral stages of high energy sources.

4 Future Prospects

We constructed the broadband transient monitor using the *Swift* BAT and the *MAXI* GSC data and made it available to the public. This work is the first attempt to analyse the BAT survey data in real-time for constructing multi-band light curves. Although the updating frequency of the light curve is still not ideal, we can now run the pipeline several times a day in real-time.

Although it varies based on the *Swift* pointing, a typical exposure time of an individual object for the BAT is roughly four hours per day (about eight hours at the highest day). Applying the BAT survey sensitivity equation described in Baumgartner et al. (2013), this typical exposure corresponds to a 5-sigma sensitivity of \sim 10 mCrab (14-195 keV). On the other hand, the daily averaged 5-sigma sensitivity of the GSC is \sim 15 mCrab in the 4-10 keV band (Sugizaki et al. 2011). Therefore, the daily sensitivity of the BAT and the GSC are comparable. Therefore, it is a good match to combine the BAT and the GSC data to monitor high energy transient sources on a daily basis.

All the *MAXI* GSC light curve data in the current broadband transient monitor is downloaded from the *MAXI*'s public web page. Since all of the light curves are created using an aperture photometry method (Sugizaki et al. 2011), the count rates in the light curves could be contaminated with bright X-ray sources located near the object. Due to a relatively poor position resolution of the GSC, if other bright X-ray source is located within 2 degrees from the object, there might be an issue in the light curve. For those sources which could be affected by nearby contaminations, we have a future plan to generate the GSC light curves of the source using the point spread function (PSF) fit method which should provide a contamination free light curve (Hiroi et al. 2011; Morii et al. 2015) using the GSC data. At the current stage, the sources which are located within 2 degrees from catalog sources in the ROSAT bright source catalog (Voges et al. 1999) with the count rate greater than 1 count s⁻¹ are flagged as possible contaminated sources at the top page of the monitor (see Table 1).

The processing time of the current pipeline is limited by the analysis of the BAT survey data. Our pipeline is processing the BAT survey data at the finest time resolution with the eight energy bands. Although we can process the data in the coarser time resolution and the smaller energy bands to speed up the process, the best spectral and temporal information can be extracted in the current

setup for the BAT data. For example, the outputs of our pipeline can provide 8 channel spectral data of the sources every five minutes when high energy sources are in the very bright state. We have a plan to process the data with multiple available computers or Graphical Processing Unit (GPU) to speed up the process.

The current broadband transient monitor contains 106 sources. However, it is not a difficult task to add sources to the monitor. We are planning to add sources based on not only the information from various observatories (e.g., the Astronomer's Telegram¹⁰, the Gamma-ray Coordinates Network¹¹) but also requests from the community.

Acknowledgments

We would like to thank the anonymous referee for comments and suggestions that materially improved the paper. This work was supported by JSPS Grant-in-Aid for Scientific Research (C) Grant Number 25400234.

References

Abdo, A. A. et al. 2011, ApJ, 736, 131

Asai, K. et al. 2015, PASJ, in press

Barthelmy, S. D., et al. 2005, Space Science Reviews, 120, 3

Baumgartner, W. H., Tueller, J., Markwardt, C. B., Skinner, G. K., Barthelmy, S., Mushotzky, R. F., Evans, P. A., Gehrels, N. 2013, ApJS, 207, 19

Esin, A. A., McClintock, J. E., Narayan, R. 1997, ApJ, 489, 865

Gehrels, N. et al. 2004, ApJ, 611, 2

Hiroi, K. et al. 2011, PASJ, 63, 677-689

Krimm, H. A. et al. 2013, ApJS, 209, 14

Keck, M.L. et al. 2015, ApJ, 806, 149

Matsuoka, M. et al. 2009, PASJ, 61, 999

Mihara, T. et al. 2011, PASJ, 63, 623

Morii, M. et al. 2015 in prep.

Nakahira, S. et al. 2010, PASJ, 62, 27

Nakahira, S. et al. 2014, PASJ, 64, 84

Sartore, N., Jourdain, E., Roques, J. P. 2015, ApJ, 806, 193

¹⁰http://www.astronomerstelegram.org

¹¹http://gcn.gsfc.nasa.gov/gcn_main.html

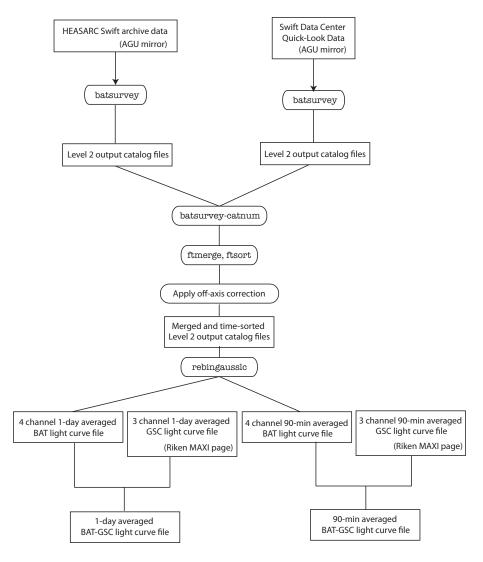


Fig. 1. Flowchart of the BAT-GSC transient monitor pipeline.

Shidatsu, M. et al. 2011, PASJ, 63, 785

Shidatsu, M. et al. 2011, PASJ, 63, 803

Sugizaki, M. et al. 2011, PASJ, 63S, S644

Tueller, J. et al. 2010, ApJS, 186, 378

Voges, W. et al. 1999, A&A, 349, 389

Yoshikawa, A. 2015, PASJ, 67, 11

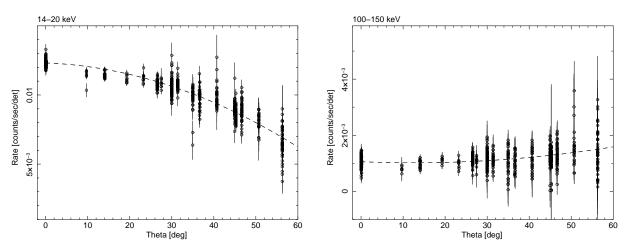


Fig. 2. The systematic trends in the BAT observed count rate of the Crab nebula as a function of the incident angle (θ) in the 14-20 keV band (left) and the 100-150 keV band (right). The dashed line is the best fit quadratic function (table 2) to the data.

Table 1. Ths source list of the broadband transient monotor

Name	R.A.	Dec.	Possible contaminated source
V709 Cas	7.2036	59.2894	
Mrk 348	12.1964	31.9570	
Gamma Cas	14.1772	60.7167	
SMC X-1	19.2714	-73.4433	T
2S 0114+650	19.5112	65.2916	
4U 0115+634	19.6330	63.7400	
CC Eri	38.5940	-43.7960	
GK Per	52.7993	43.9047	
BQ Cam	53.7495	53.1732	
X Per	58.8462	31.0458	
LSV+44 17	70.2470	44.5300	
LMC X-4	83.2075	-66.3705	T
Crab Nebula Pulsar	83.6332	22.0145	
1A 0535+262	84.7274	26.3158	
LMC X-3	84.7342	-64.0823	T
NGC 2110	88.0474	-7.4562	
4U 0614+091	94.2804	9.1369	
MXB 0656-072	104.5703	-7.2105	
EXO 0748-676	117.1388	-67.7500	
Vela Pulsar	128.8361	-45.1764	
GS 0834-430	128.9790	-43.1850	
Vela X-1	135.5286	-40.5547	
MCG -05-23-016	146.9173	-30.9489	
GRO J1008-57	152.4417	-58.2917	
NGC 3227	155.8774	19.8651	T
Mrk 421	166.1138	38.2088	
NGC 3516	166.6979	72.5686	
XTE J1118+480	169.5450	48.0370	
Cen X-3	170.3158	-60.6230	T
NGC 3783	174.7572	-37.7386	
1E 1145.1-6141	176.8692	-61.9539	

Table 1. (Continued)

NGC 4151	182.6357	39.4057	
GX 301-2	186.6567	-62.7706	
3C 273	187.2779	2.0524	
GX 304-1	195.3217	-61.6019	
Cen A	201.3651	-43.0191	
4U 1323-619	201.6504	-62.1361	
IC 4329A	207.3303	-30.3094	
NGC 5506	213.3119	-3.2075	
PSR B1509-58	228.4813	-59.1358	
Cir X-1	230.1703	-57.1667	
H 1538-522	235.5971	-52.3861	
1E 1547.0-5408	237.7255	-54.3066	
H 1553-542	239.4512	-54.4150	
4U 1608-522	243.1792	-52.4231	T
Sco X-1	244.9795	-15.6402	
SWIFT J1626.6-5156	246.6510	-51.9428	T
4U 1624-490	247.0118	-49.1985	
4U 1626-67	248.070	-67.4619	
4U 1636-536	250.2313	-53.7514	
GX 340+0	251.4488	-45.6111	
GRO J1655-40	253.5006	-39.8458	T
Her X-1	254.4576	35.3424	T
OAO 1657-415	255.1996	-41.6731	T
XTE J1701-407	255.4349	-40.8583	T
GX 339-4	255.7063	-48.7897	
GX 349+2	256.4354	-36.4231	T
4U 1705-440	257.2270	-44.1020	T
4U 1722-30	261.8883	-30.8019	T
GX 9+9	262.9342	-16.9617	
4U 1728-34	262.9892	-33.8347	
GX 1+4	263.0090	-24.7456	T
MXB 1730-335	263.3504	-33.3877	
SLX 1735-269	264.5667	-27.0044	T

Table 1. (Continued)

)				
	4U 1735-44	264.7429	-44.4500	
	SGR A Gal center complex	266.4168	-29.0078	
	2E 1742.9-2929	266.5229	-29.5153	
	XTE J17464-3213	266.5650	-32.2335	T
	GX 3+1	266.9833	-26.5636	
	SWIFT J1753.5-0127	268.3679	-1.4525	
	GX 5-1	270.2842	-25.0792	T
	GX 9+1	270.3846	-20.5289	
	SAX J1808.4-3658	272.1150	-36.9790	
	XTE J1810-189	272.6079	-19.0700	
	SAX J1810.8-2609	272.6850	-26.1500	
	GX 13+1	273.6315	-17.1574	
	GX 17+2	274.0058	-14.0364	T
	4U 1820-30	275.9186	-30.3611	
	4U 1822-371	276.4450	-37.1053	
	Ginga 1826-24	277.3675	-23.7969	
	XB 1832-330	278.9338	-32.9914	
	Ser X-1	279.9896	5.0358	
	Ginga 1843+00	281.4125	0.8917	
	4U 1850-086	283.2703	-8.7057	
	V1223 Sgr	283.7593	-31.1635	
	XTE J1855-026	283.8804	-2.6067	
	XTE J1856+053	284.1786	5.3094	
	HETE J1900.1-2455	285.0360	-24.9205	
	SWIFT J1910.2-0546	287.5950	-5.7990	
	Aql X-1	287.8167	0.5850	
	SS 433	287.9565	4.9827	
	GRS 1915+105	288.7983	10.9456	
	4U 1916-053	289.6995	-5.2381	
	SWIFT J1922.7-1716	290.6542	-17.2842	
	4U 1954+31	298.9264	32.0970	
	Cyg X-1	299.5903	35.2016	
	Cygnus A	299.8682	40.7339	

Table 1. (Continued)

V404 Cyg	306.0159	33.8672	
EXO 2030+375	308.0633	37.6375	
Cyg X-3	308.1074	40.9578	
SAX J2103.5+4545	315.8990	45.751	
Ginga 2138+56	324.8780	56.9861	
Cyg X-2	326.1717	38.3217	
NGC 7172	330.5080	-31.8698	T
4U 2206+54	331.9843	54.5185	
II Peg	358.7669	28.6337	

Table 2. Best fit equations between the BAT Crab count rate and the incident angle θ .

Energy band	Best fit quadratic equation	
14-20 keV	Rate = $0.0123169 - 1.15218 \times 10^{-5} \theta - 1.4965 \times 10^{-6} \theta^2$	
20-24 keV	$\mathrm{Rate} = 0.0066923 + 6.10315 \times 10^{-6} \theta - 6.78433 \times 10^{-7} \theta^2$	
24-35 keV	$\mathrm{Rate} = 0.0105085 + 5.19742 \times 10^{-6} \theta - 6.91427 \times 10^{-7} \theta^2$	
35-50 keV	$\mathrm{Rate} = 0.0069828 + 7.88677 \times 10^{-6} \theta - 5.25433 \times 10^{-7} \theta^2$	
50-75 keV	$\mathrm{Rate} = 0.0057086 + 4.41883 \times 10^{-6} \theta - 2.67754 \times 10^{-7} \theta^2$	
75-100 keV	$\mathrm{Rate} = 0.0020645 + 8.86035 \times 10^{-7} \theta + 5.79986 \times 10^{-8} \theta^2$	
100-150 keV	$\mathrm{Rate} = 0.0010577 - 6.27195 \times 10^{-6} \theta + 2.51476 \times 10^{-7} \theta^2$	
150-195 keV	${\rm Rate} = 0.0001824 - 3.96457 \times 10^{-6} \theta + 1.74441 \times 10^{-7} \theta^2$	

Table 3. Products of the broad-band transient monitor

Plots of daily seven channel light curves and the hardness ratio between the BAT 50-100 keV and the GSC 2-5 keV band

Plots of zoom-in daily light curves over the last ten days and the hardness ratio between the BAT 50-100 keV and the GSC 2-5 keV band

Interactive plots of daily seven channel light curves and the hardness ratio between the BAT 50-100 keV and the GSC 2-5 keV band

Plots of 90 minutes seven channel light curves

Plots of zoom-in 90 minutes seven channel light curves over the last 10 days

FITS light curve files of BAT four channel daily light curves

FITS light curve files of BAT four channel 90 minutes light curves

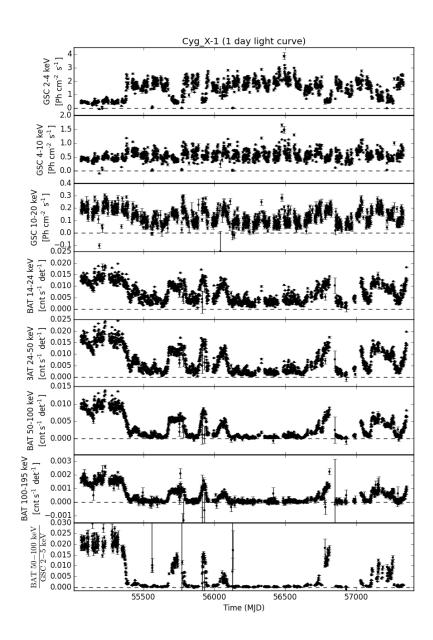


Fig. 3. Daily averaged broadband light curve of Cyg X-1. A clear hard-to-soft state transition is visible at MJD 55300 and also the short soft-to-hard and hard-to-soft state transitions are visible at MJD 55700, 55900 and 56800.

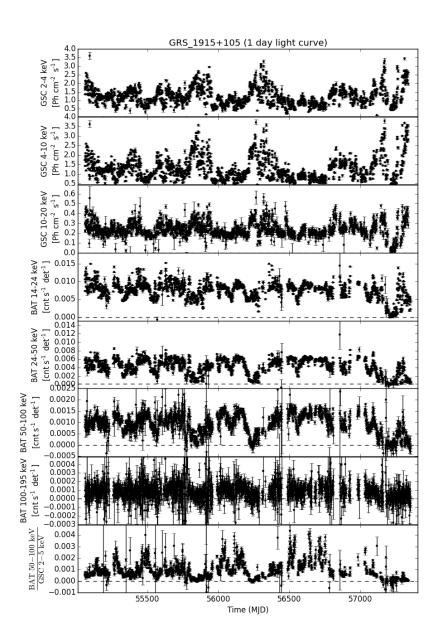


Fig. 4. Daily averaged broadband light curve of GRS 1915+105. Several hard-to-soft state transitions are clearly visible in MJD 55700, 56300 and 57200.

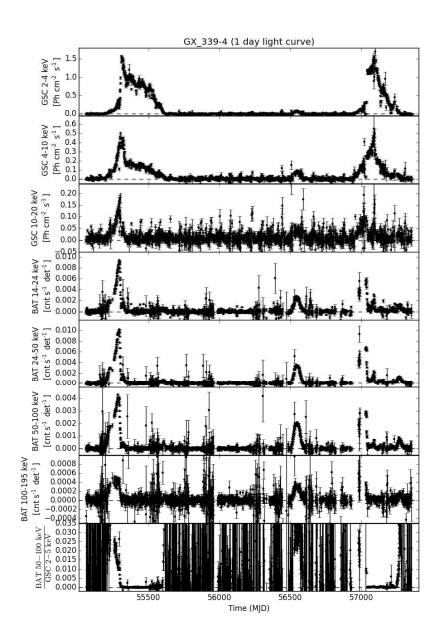


Fig. 5. Daily averaged broadband light curve of GX 339-4. During the outburst around MJD 55200, the hard-to-soft spectral evolution at the tail part of its outburst is evident between the GSC 2-4 keV and BAT 50-100 keV band.

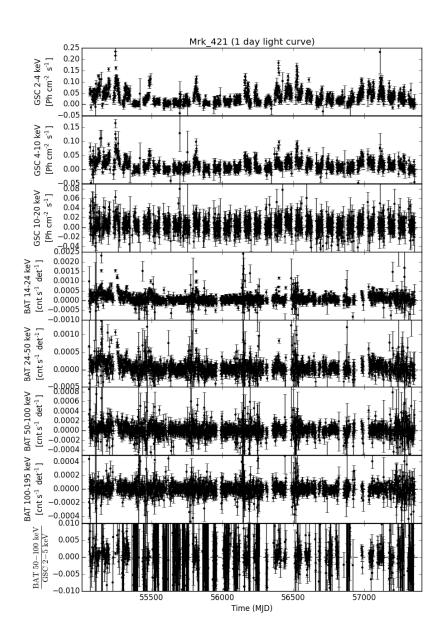


Fig. 6. Daily averaged broadband light curve of Mrk 421. The hard X-ray emission is detected by the BAT data during the outburst episodes such as MJD 55250 and 55800.

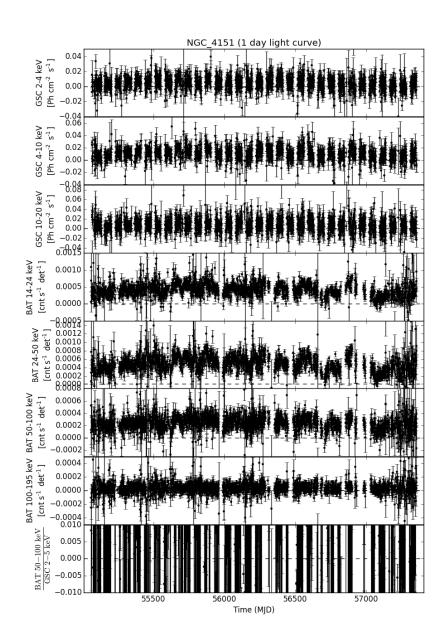


Fig. 7. Daily averaged broadband light curve of NGC 4151. The variable emission from NGC 4151 is clearly visible in the hard X-ray bands rather than the soft X-ray bands.

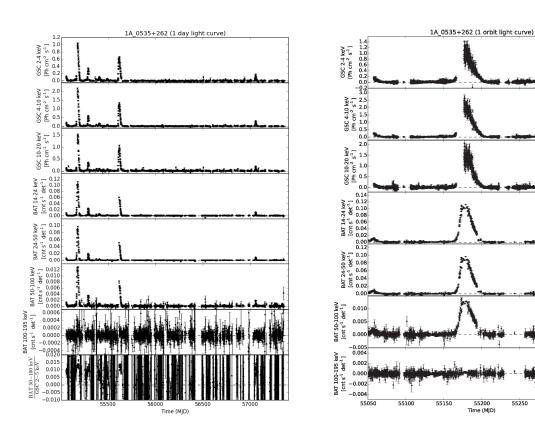


Fig. 8. Daily (left) and 90-minutes averaged (right) broadband light curve of AO535+262. The outbursts are clearly visible up to 100 keV. Moreover, since the outburst emission is so intense, the temporal profile is clearly resolved in 90-minutes averaged light curve.

55250

55300